J. Fluid Mech. (1978), *vol.* 88, *part* 3, *pp.* 585–608
Printed in Great Britain

Structural similarity in radial correlations and spectra of longitudinal velocity fluctuations in pipe flow

By K. J. BULLOCK, R. E. COOPER
Department of Mechanical Engineering, University of Queensland, St Lucia, Queensland 4067
AND F. H. ABERNATHY
Division of Applied Sciences, Harvard University, Cambridge, Massachusetts 02138

(Received 4 March 1977 and in revised form 2 May 1978)

The paper describes correlation measurements in both broad and narrow frequency bands of the longitudinal velocity fluctuations in fully developed pipe flow at four positions for a reference probe whilst a second probe was traversed radially from deep in the sublayer to a position near the axis with both longitudinal and transverse separations zero ($\Delta x = \Delta z = 0$). Such measurements require that both the Covariant (Co) and Quadrature (Quad) correlations be determined for each of the 15 frequencies used to constrain the wave component λ_x.

The new data demonstrate that low frequency, large scale turbulence fluctuations extend over the majority of the radial region and that these components are highly correlated. By using a similarity variable $k_x y$, along with a normalized wall distance y/y_{REF}, both correlation functions, i.e. the Co and the Quad components, are shown to collapse. The physical significance of this is discussed.

The broad-band data do not collapse because of the large range of wave sizes. However, the present experiment does show that strong radial correlations exist even when one probe is at $y^+ = 1$. This conflicts with the earlier data of Favre, but agrees with the more recent work of Comte-Bellot. There is a significant amount of turbulent energy in frequencies less than 16 Hz ($\omega^+ = 0{\cdot}008$) for turbulent flows of about 10^5 Reynolds number.

The spectral function $\omega\Phi(\omega)$ is also presented for a range of y^+ values. Using this form for the power spectral density, along with the stochastic wave modelling and similarity arguments of this paper, it is shown how a consistent explanation for the behaviour of these spectra is obtained. In addition some preliminary results from cross-spectral analyses are presented and suggestions made as to their physical significance.

1. Introduction

Further experiments in turbulent pipe flow are described and structural interpretations given. The work involved extensive radial correlations both broad-band and frequency filtered and also the computation of various spectral functions of the longitudinal component u. Earlier work in the Department involved measurements of correlations of the u component in frequency bands with longitudinal or transverse spatial separations. Fourier transformation of these data produced two-dimensional power spectral densities at a particular y^+ location. Morrison & Kronauer (1969)

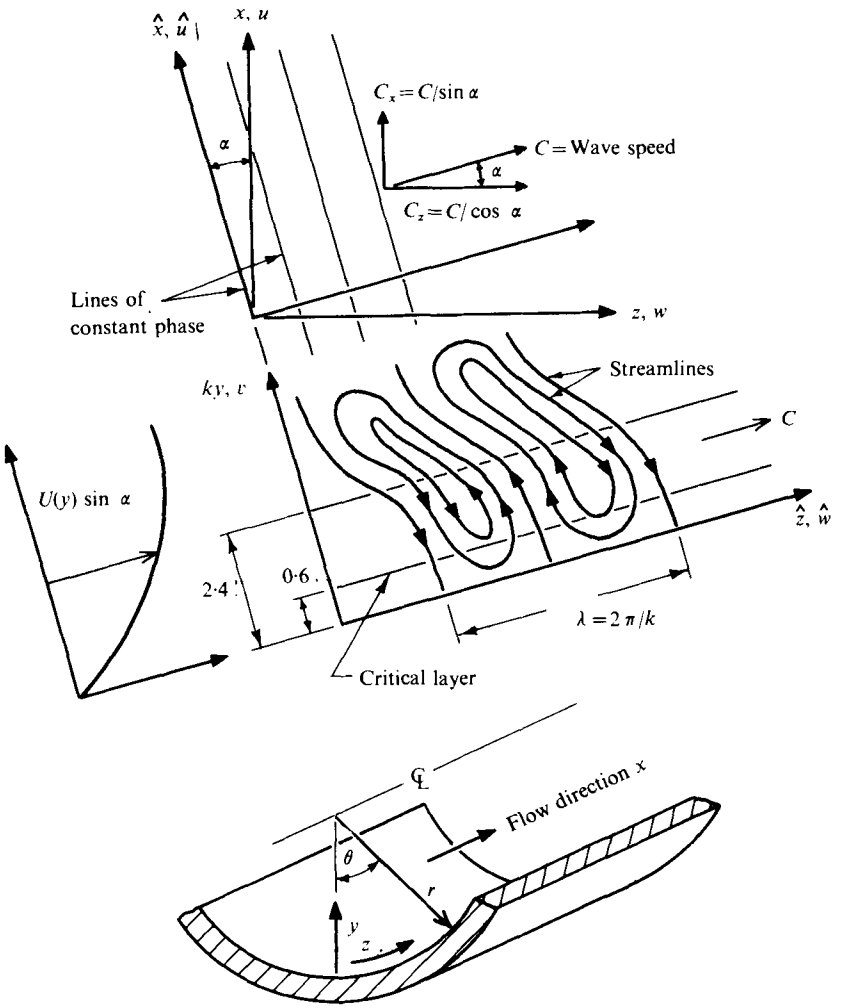

FIGURE 1. Pipe co-ordinates and wave schematic diagram.

presented contour plots of these functions for a wide range of y^+ and shear velocities U_τ. They successfully interpreted their data in the light of a stochastic wave model of turbulence with co-ordinates as specified in figure 1. These co-ordinates are simply the result of rotating the x, z plane about the y axis through an angle α so that the (new) $y, \hat{z}$ plane is perpendicular to the wave fronts or lines of constant phase. Because of the symmetrical distribution of wave power in k_z, right and left handed helical waves are equally strong. In the new co-ordinates, the measurable turbulent components are

$$u = \hat{u}\cos\alpha + \hat{w}\sin\alpha$$

and

$$w = \hat{w}\cos\alpha - \hat{u}\sin\alpha.$$

They also proposed a scaling or similarity variable which requires turbulence features to collapse on wavenumber and wall distance as a product term ky, where

$$k^2 = k_x^2 + k_z^2 \quad \text{and} \quad \alpha = \tan^{-1} k_x/k_z.$$

This allows the two-dimensional power plots to be written

$$\mathscr{P}(\omega^+, k^+y^+) = f(k^+y^+)\, A(\omega^+, k_z^+), \tag{1}$$

where f is the 'wave intensity function' and A is 'wave strength'. These authors also laid the foundations for a mathematical treatment of the similarity theory in the appendix of their paper. In line with the Morrison & Kronauer presentation, Reynolds scaling has been used throughout this paper and hence the non-dimensional variables are

$$y^+ = yU_\tau/\nu, \quad k^+ = k\nu/U_\tau, \quad \omega^+ = \omega\nu/U_\tau^2,$$

where U_τ is the usual shear velocity. In the recent work of McConachie, Bullock & Kronauer (1977) the three-dimensional spectral function $\Phi(k_x, k_z, \omega)$ has been obtained at a particular y^+. This has led to an accurate definition of convection velocity C_x as a function of wave size and similarity is substantially verified.

Favre, Gaviglio & Dumas (1957, 1958, 1967) and Sabot & Comte-Bellot (1972) present contours of correlations with optimal time delay. Grant (1958) and Comte-Bellot (1969) made space–time correlation measurements of all three velocity components in a boundary layer. The structural interpretation of time-delayed correlations and data in the untransformed variables is difficult.

Recent work by Perry & Abell (1975) shows that the similarity variable correlates the turbulent intensity (strictly a two-point correlation) across the flow. Their work extends to one-dimensional spectra and an excellent similarity collapse is obtained. Their paper is particularly significant as it demonstrates that the true similarity region (i.e. where ky scaling is applicable) can be expected only between $y^+ \simeq 70$–100 and $y/a = 0{\cdot}1$, a feature also implied by Bradshaw (1971). Our experience indicates that the region $y^+ = 50$ to $y/a = 0{\cdot}2$–$0{\cdot}3$ shows good similarity. This limited range means that low Reynolds number turbulence will probably not show similarity in the sense in which the term is used in this paper. Hence, care is needed in suggesting generalized theories from studies of low Reynolds number flows. There is evidence of a change in the turbulent structure at a low Reynolds number of about 30 000 (Morrison *et al.* 1971). These authors were investigating two-dimensional spectra of the sublayer.

Elliott's (1972) atmospheric boundary-layer data indicate that not only u but also v and w show trends in agreement with Morrison & Kronauer's (1969) hypothesis. The v component is independent of wave angle α since wave propagation is in a plane orthogonal to y, the direction of v components (see figure 1). Hence, it is the only component which by itself can be used to test the similarity hypothesis but unfortunately, it is also the hardest to measure close to a surface (McConachie & Bullock 1976).

Tritton (1967) carried out extensive correlation measurements as functions of several combinations of all spatial arguments and time. Again, the use of untransformed variables renders interpretation difficult, but he deduced that the similarities between the wall and outer regions are more marked than the differences and that the description of the large eddies in the wall region as a coherent eruption from the viscous sublayer is unsatisfactory.

2. Data collection

The data on which this paper is based were taken twice because the initial set showed effects which were at variance with similar previous results, notably Favre *et al.* (1957, 1958). Hence the original experiment was expanded and refined using different experimental equipment and an alternative technique of data analysis. Identical results were obtained.

Generation of the correlations (both broad-band and frequency filtered) involved stationing two probes to measure u fluctuations in a circular tube. The probes were positioned at the same x and z locations and separated in the radial direction y. The probe arrangement and mechanism were similar to those described by Morrison (1969).

Flow Corporation anemometers were used (type CTA) and operated in constant temperature mode (resistance ratio 1·5). Wires were 2·5 μm diameter tungsten, 0·5 mm long. The wires were checked for straightness, parallelism and run-out on optical equipment in the Department's Metrology Laboratory before being installed in the tunnel.

The d.c. outputs of the anemometers were used, ensuring that all low-frequency energy was retained. The fluctuating parts of the signals were then amplified with Preston wide band (10 kHz) floating differential amplifiers (model 8300 H) to bring them to acceptable levels for recording on the Hewlett–Packard F.M. 14-channel tape deck (model no. 3955 C). Recording speed was 1·52 m/s (60 in./s). This speed was chosen so that correlation fidelity (i.e. phase shift less than 1·5° between channels and negligible distortion on any one channel) could be maintained to 5 kHz. On each channel, the frequency response was from d.c. to 20 kHz. Hot-wire and equipment performance were monitored continuously.

Using a friction velocity U_τ of 0·61 m/s (2·0 ft/s), three reference y^+ values were chosen, viz. 50, 100 and 300, and approximately 15 secondary y^+ values about each reference, defining the correlations from $y^+ = 1$ out to $y^+ = 1500$ ($y/a = 0{\cdot}57$). Some correlations were also taken around a reference y^+ of 20. The tube diameter is 133·4 mm (5·25 in.).

3. Data processing

In line with most previous work in the Departmental laboratories, analog cross-spectral density techniques have been used rather than real-time correlation analyses. The correlation function $R(\tau, \Delta x, \Delta z, y_1, y_2)$ and the cross-power spectral density function $\Phi(\omega, k_x, k_z, y_1, y_2)$ are of course a Fourier transform pair and neither contains more information than the other. However, our experience when dealing with broad-band turbulence data has been that more accurate results are obtained if at least one of the troublesome Fourier transformation operations is by-passed, i.e. the time delay/frequency transformation. A further compelling reason for remaining in frequency/wavenumber space is contained in the product decomposition of equation (1). This corresponds to a convolution in the space–time domain, and it is extremely unlikely that any such relation would have been discovered (Morrison & Kronauer 1969). Furthermore, the spectral/wavenumber treatment leads on to the advanced theory of wave–wave interactions, the mechanism by which the whole equilibrium structure is maintained. This is expressed mathematically by the nonlinear terms in the Navier–Stokes equations.

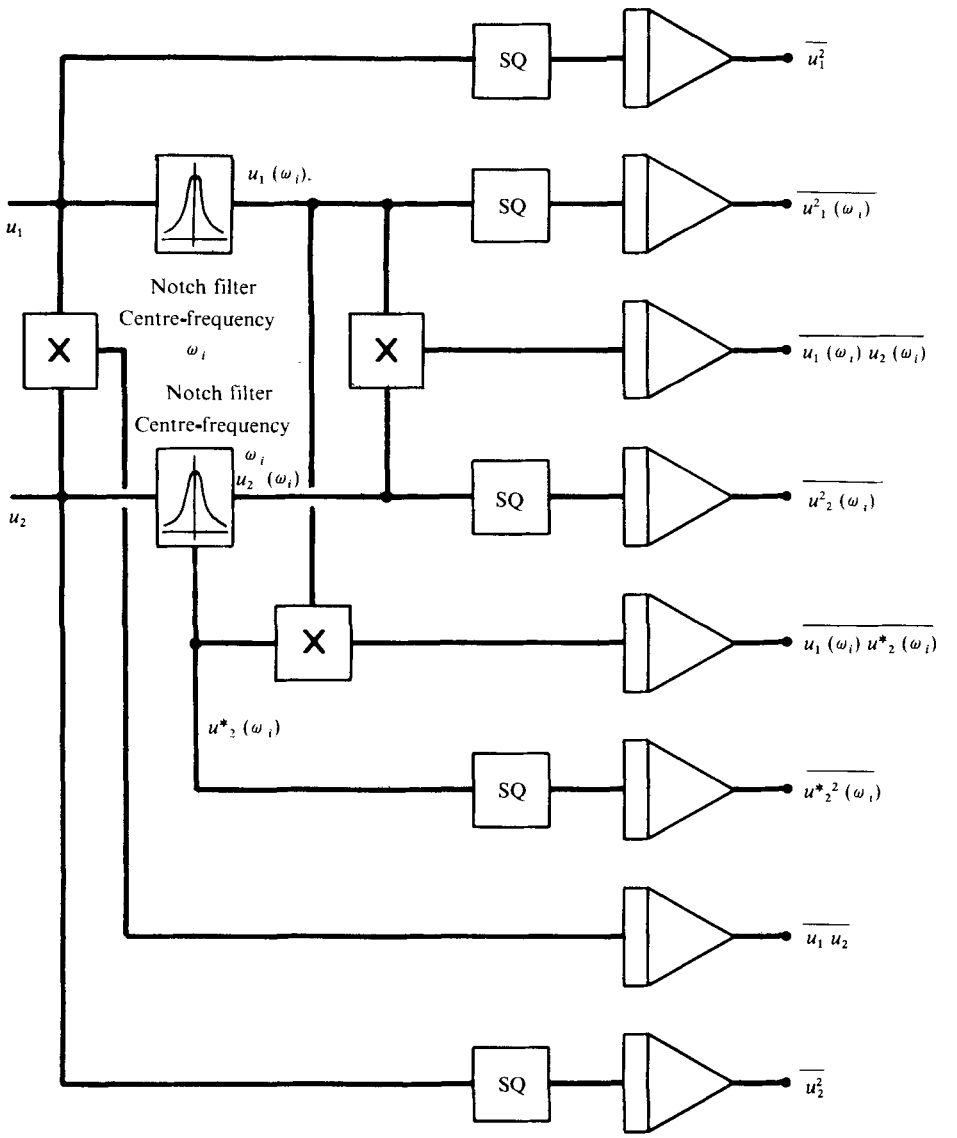

FIGURE 2. Analog correlation circuit.

However, this paper is concerned with the radial correlations only and rather than expand in the eigenfunctions of y as described by Lumley (1970), we have chosen to present the Co and Quad correlations for various frequencies. The data analysis was carried out on an EAI 231R analog computer. The analog components have been discussed by Morrison (1969) and acceptable accuracy is obtained from d.c. to 8 kHz. Broad-band and narrow-band correlations were computed by circuits such as the one shown in figure 2 where u_1 and u_2 are the two hot-wire turbulence signals. The analog notch filters are second-order active systems with transfer functions giving effective band-widths of 20 % for all except the lowest of the centre-frequencies.

The correlation coefficients are calculated from the following formulae:

$$R_{uu}(y_1, y_2) = \frac{\overline{u(y_1) \cdot u(y_2)}}{\{\overline{u^2(y_1)} \cdot \overline{u^2(y_2)}\}^{\frac{1}{2}}} \quad \text{(broad band)}, \tag{2}$$

$$R_{uu}(y_1, y_2, \omega_i) = \frac{\overline{u(y_1, \omega_i) \cdot u(y_2, \omega_i)}}{\{\overline{u^2(y_1, \omega_i)} \cdot \overline{u^2(y_2, \omega_i)}\}^{\frac{1}{2}}} \quad \text{(narrow band Co)}, \tag{3}$$

$$R_{uu}(y_1, y_2, \omega_i) = \frac{\overline{u(y_1, \omega_i) \cdot u^*(y_2, \omega_i)}}{\{\overline{u^2(y_1, \omega_i)} \cdot \overline{u^{*2}(y_2, \omega_i)}\}^{\frac{1}{2}}} \quad \text{(narrow band Quad)}, \tag{4a}$$

where

$$u^*(y_2, \omega_i) = -iu(y_2, \omega_i). \tag{4b}$$

The correlation magnitude and phase are given by

$$M_{uu}(y_1, y_2, \omega_i) = [R^2_{uu}(y_1, y_2, \omega_i) + R^{*2}_{uu}(y_1, y_2, \omega_i)]^{\frac{1}{2}} \tag{5}$$

and

$$\theta_{uu}(y_1, y_2, \omega_i) = \tan^{-1} \frac{R^*_{uu}(y_1, y_2, \omega_i)}{R_{uu}(y_1, y_2, \omega_i)}. \tag{6}$$

In future we shall use a simpler notation, e.g.

$$R_{u_1 u_2}(\omega_i) = R_{uu}(y_1, y_2, \omega_i).$$

Two-point velocity correlations such as $R_{u_1 u_2}(\tau)$ are not symmetric functions of τ because the flow is non-homogeneous in y and thus the frequency transform is complex. Hence both the real part or in phase component of $M_{u_1 u_2}(\omega_i)$ (the Covariant or Co-correlation) and the imaginary part or out of phase component of $M_{u_1 u_2}(\omega_i)$ (the Quadrature or Quad-correlation) must be measured separately at each pair of displacements and for each frequency ω_i. The Quad-correlation is measured by shifting the phase of the filtered velocity signal $u_2(\omega_i)$ by 90 degrees ($u_2^*(\omega_i)$) and correlating with the unshifted $u_1(\omega_i)$ signal as indicated in (4*a*). For second-order filters the 90 degree phase shifted signal can be conveniently taken from the output of the second integrator in the filter circuit. The transfer function of this portion of the circuit is not ideal and shows some response at d.c., namely 18 db down. Hence care is needed to remove any d.c. bias from the signals but at the same time preserve all significant low frequency energy. To achieve this, high-pass input filters with a 0·08 Hz corner frequency were used.

For the analysis described here, a bank of five pairs of filters plus the broad-band circuitry was used, and by replaying the tape deck at 152, 86 and 38 cm/s successively, 15 frequencies embracing all significant energy were analysed.

The power spectral density $\Phi(\omega)$, defined by

$$\Phi(\omega) = \Phi_{u_1 u_1}(\omega) = \int_{-\infty}^{\infty} R_{u_1 u_1}(\tau) \exp(-i\omega\tau)\, d\tau, \tag{7}$$

was determined from the filtered signals after calibration with a known spectrum following Walker (1971). The modified form of the power spectral density $\omega\Phi(\omega)$ or $f\Phi(f)$ has been used in this paper because when the ordinate scale is linear, changes in spectral content and shape are more readily discernible and the area between any two abscissae on a logarithmic scale is the fraction of total signal energy contained between those two frequencies. The total area under the curve for normalized spectra must equal unity, providing a sensitive check on the accuracy of the analysis.

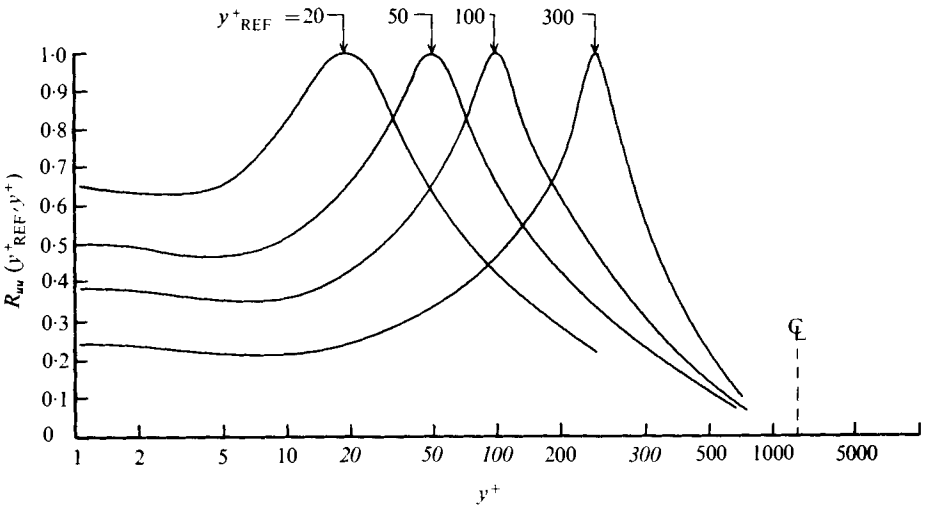

FIGURE 3. Broad-band correlations.

	Tape speed					
	152 (cm/s)		76 (cm/s)		38 (cm/s)	
	f (Hz)	ω^+	f (Hz)	ω^+	f (Hz)	ω^+
Effective filter frequencies	0·5	0·00025	1	0·00049	2	0·00098
	3	0·0015	6	0·003	12	0·0059
	18	0·0089	36	0·018	72	0·035
	108	0·053	216	0·11	432	0·212
	648	0·32	1296	0·64	2592	1·27

TABLE 1

The magnitude of the cross-power spectral density function is given by

$$\omega_i G_{u_1 u_2}(\omega_i) = \frac{M_{u_1 u_2}(\omega_i)}{R_{u_1 u_2}} [\omega_i \Phi_{u_1 u_1}(\omega_i) . \omega_i \Phi_{u_2 u_2}(\omega_i)]^{\frac{1}{2}}. \tag{8}$$

The phase of the correlation function, (6), is the same as that of the cross-power spectral density function. The normalization used in (8) ensures that the area under the $\omega G_{u_1 u_2}(\omega)$ versus $\log \omega$ curves is unity (figure 13).

The frequencies of the analysis are shown in table 1, the first column being the real frequencies of the filters and the other frequencies being obtained by tape-deck speed changes.

The proportional band-width ($B_p = \pi\zeta$) of the 0·5 Hz filter was 50 %; for all other filters it was set at 20 %. With 200 s integration time the standard error is 10 % for the lowest frequency filter. Testing showed this to be an upper bound on the error. Typical errors for all other filters were a fraction of one per cent.

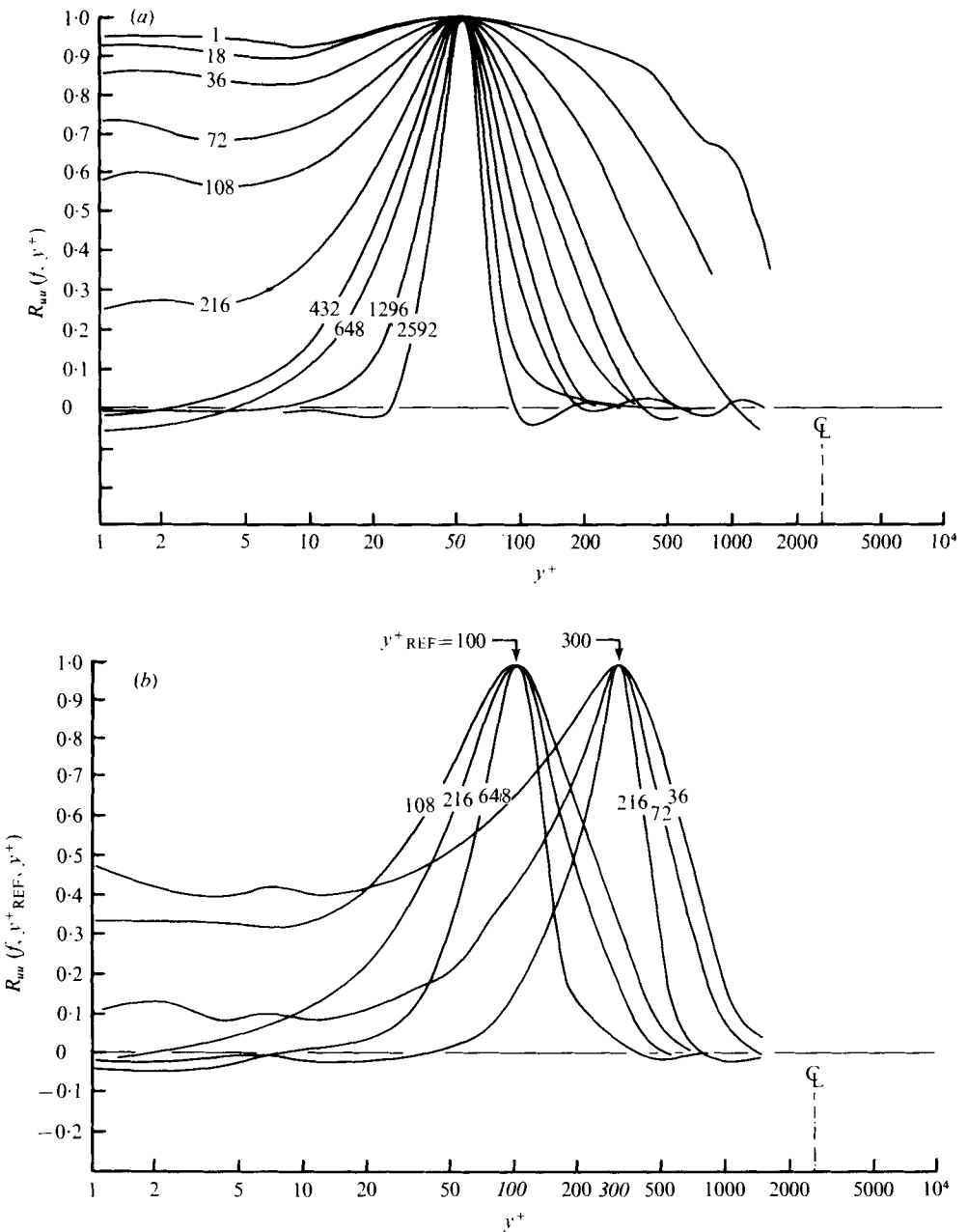

FIGURES 4 (*a*, *b*). For legend see facing page.

4. Some new two-point correlations

The broad-band correlations were presented in figure 3 while various sets of the filtered functions are shown in figures 4 (*a*), (*b*) and (*c*).

The broad-band correlation functions in figure 3 indicate that a substantial level of correlation exists throughout the shear layer in pipe flow, significantly higher than that reported by Favre *et al.* (1957, 1958) for flat plate boundary layers. Except for the

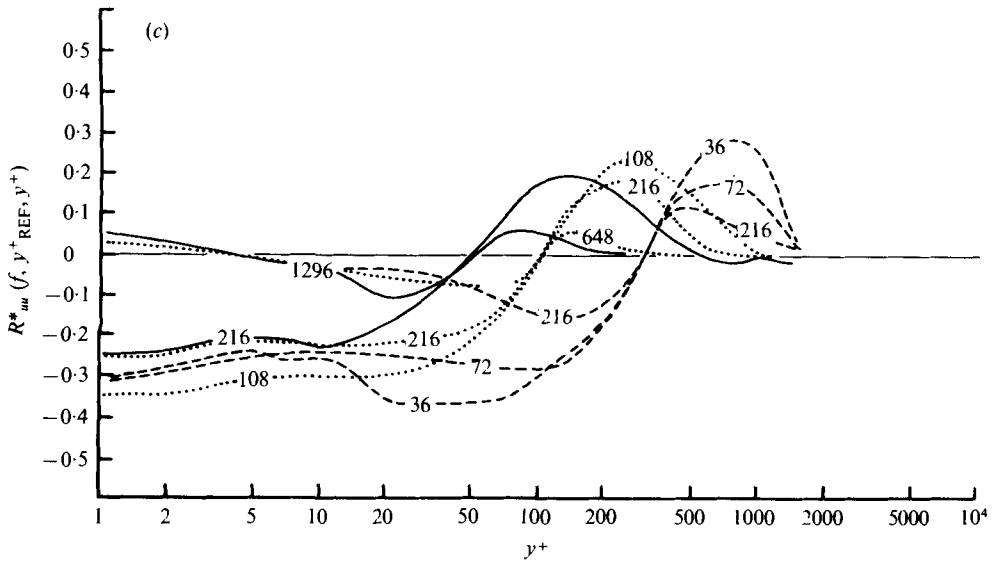

FIGURE 4. (*a*) Filtered Co-correlations for $y^+_{REF} = 50$. Filtering frequencies as marked (Hz).

f (Hz)	ω^+	f (Hz)	ω^+
1	0·00491	216	0·106
18	0·00885	432	0·212
36	0·0177	648	0·318
72	0·0354	1296	0·637
108	0·0531	2592	1·274

(*b*) Filtered Co-correlations for $y^+_{REF} = 100$ and 300. Filtering frequencies as marked (Hz).

f (Hz)	ω^+	f (Hz)	ω^+
36	0·0177	216	0·106
72	0·0354	648	0·318
108	0·0531		

(*c*) Filtered Quad-correlations for $y^+_{REF} = 50$, 100 and 300. Filtering frequencies as marked (Hz).

y^+_{REF}	f (Hz)	ω^+
300 – – –	36	0·0177
100	72	0·0354
50 ——	108	0·0531
	216	0·106
	648	0·318
	1296	0·637

region $y^+ < 5$, where the correlations are independent of y^+, it is not possible to define the conventional flow regions of buffer layer, log region, etc., from the behaviour of the correlation coefficients with y^+. The reason for the high broad-band correlation coefficients is evident when the correlation data are presented as a function of frequency (figures 4 (*a*), (*b*), (*c*)). Figure 4 (*a*) contains data covering the entire frequency range and is typical of the data available at y_{REF} of 100, and 300 for which only a subset is presented in figure 4 (*b*). The Co-correlation values for $f = 1$ Hz, $y^+ = 1$ and $y^+_{REF} = 20, 50$, 100 and 300 are 0·96, 0·95, 0·92 and 0·84 respectively, and the Quad-correlations are measured at less than 0·1. The low frequency components are highly correlated and in phase or nearly so over most of the 'boundary layer'. As the frequency increases the

total correlation $M_{u_1 u_2}(\omega)$ falls off and the phase angle begins to become noticeable as y separation increases. There is no sharp boundary between the low frequency and intermediate frequency behaviour; however, for purposes of discussion 36 Hz can be used as a boundary. At 36 Hz there is a noticeable phase for $y^+_{\mathrm{REF}} = 300$ as shown by the Quad values in figufe 4 (*c*). At the same frequency but $y^+_{\mathrm{REF}} = 50$, the Co is 0·85 and the Quad is of the order of $-0{\cdot}05$ at $y^+ \leqslant 10$.

These observations imply that the inner regions of the boundary layer are highly correlated with *each other* and are in phase, i.e. high Co and low Quad-correlation, especially over the lower frequency portion of the spectrum. It appears that the longitudinal velocity $u(y,t) = A(t)f(y)$, especially for the low frequencies. Previous experimental evidence for this view is contained in Abernathy's boundary-layer film (1969), where it can be seen that the velocity profile in the sublayer region appears as a straight line with time-varying slope. Additionally, Grass (1971) noted that the instantaneous velocity profiles seemed to oscillate randomly about some average profile. Oscillations did not take the form of local spikes on the mean profiles, but exhibited strong correlations over large portions of the visible flow depth.

The Quad-correlations for the lowest frequencies are not presented in figure 4 (*c*) because they are generally of low magnitude. However, the Quad at $f = 36$ Hz for $y^+_{\mathrm{REF}} = 300$ is roughly constant at about 0·35 for $y^+ < 50$ and the Co-correlation is approximately 0·43 for this region. It may be that this portion of the shear layer ($y^+ < 50$ and $f < 36$ Hz) is responding to large scale log-layer fluctuations. Leslie (1973) commented from a fundamental consideration of the Navier–Stokes equations that the log-layer is a self-consistent, self-sustaining turbulent phenomenon calculable without reference to the inner (viscous) and outer flows into which it must merge in any real situation. Hence, the sublayer can be thought of simply as the necessary boundary conditions on the velocity components. In this frequency regime the sublayer is being driven by the outer flow; nevertheless there may still be a feedback mechanism operating between the inner and outer layers, the coupling being provided by the momentum interchange process. However on physical and experimental grounds (e.g. rough and smooth wall log-region velocity profiles are expressible by a single equation) it may be argued that the coupling probably decreases as Re increases. If the properties of one region are changed, the entire coupled process can be significantly altered. The drag reduction property of dilute solutions of long chain polymers in water is an example where changes in the sublayer response affect the flow, as noted by Paterson & Abernathy (1972) and Bertschy & Abernathy (1977). The viscosity of polymer solutions is strongly strain rate dependent. Thus the kinematic viscosity of the sublayer is increased while that of the bulk of the fluid is essentially unchanged.

The next frequency range of interest in the correlations extends from $f > 36$ Hz to $f \approx 400$ Hz. Again the frequency boundary is not well-defined but is characterized by a significant decrease in the Co and an increase in the magnitude of the Quad-correlations with lateral separation of the measuring points. It should be noted that the sign of the Quad-correlations in figure 4 (*c*) is such that the signal at the outer y^+ station leads that of the measuring point closest to the wall. Momentum interchange between the inner and outer flow would involve stretching of fluid elements and is consistent with this observation. Indeed the spectral measurements of Bremhorst & Walker (1973) show that the major portion of the $\overline{uv}$ energy is concentrated in this frequency band throughout the 'boundary layer'.

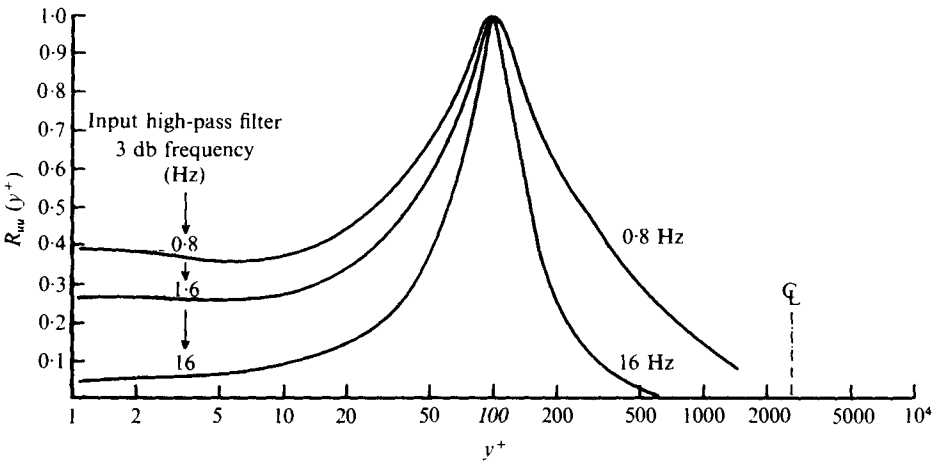

FIGURE 5. Effect of input filter cut-off frequency on broad-band correlations around $y^+_{REF} = 100$.

The correlation data presented in figures 3 and 4 differ significantly from those generated by Favre *et al.* (1957, 1958). Favre's data fall off steeply to values of 0·1 near the wall. Figure 4 shows, on the other hand, significant asymptotic values of the correlations as the wall is approached. Favre's experiments were in a flat plate boundary layer and not in fully developed pipe flow. Tritton (1967), however, concluded that his experiments gave no indication of any difference in the large eddy structure in the wall regions of boundary-layer and channel flow turbulence. Hence, it seems possible that Favre's data did not extend to low enough frequencies and so contributions from these well-correlated components have been lost. The effect of higher cut-offs in the input high-pass filter is shown in figure 5. The present data agree with those of Comte-Bellot (1969) in channel flow.

5. Collapse of the data

The two-point space–time correlation description of a general turbulent flow field involves functions of the six dependent variables (*uu*, *uv*, *vw*, etc.) in the eight independent variable space. Hence the *uu* correlation with full arguments would be

$$R_{u_1 u_2} = R_{uu}(x_1, x_2, y_1, y_2, z_1, z_2, t_1, t_2). \tag{9}$$

However, in fully developed turbulent pipe flow stationarity in time (t) and homogeneity in the two spatial variables x and z allow the use of increments rather than absolute values, viz.

$$x_2 - x_1 = \Delta x,$$

$$z_2 - z_1 = \Delta z$$

and

$$t_1 - t_2 = \Delta t = \tau.$$

Hence,

$$R_{u_1 u_2} = R_{uu}(\Delta x, y_1, y_2, \Delta z, \tau). \tag{10}$$

In the present experiments $\Delta x = \Delta z = 0$ and so

$$R_{u_1 u_2} = R_{uu}(y_1, y_2, \tau). \tag{11}$$

Frequency filtration automatically generates functions in the transform of the time variable, viz. ω. Therefore

$$R_{u_1 u_2} = R_{uu}(y_1, y_2, \omega), \tag{12}$$

and is the experimentally determined spectral correlation coefficient.

Morrison & Kronauer (1969) showed that frequency filtering constrains k_x. The convection velocity C_x is approximately equal to the local mean velocity in the log and outer flow regimes in fully developed turbulent pipe flow and $k_x = \omega/C_x$. Any variation in C_x is small when compared with the three orders of magnitude in the energy spectrum of u. It is required by similarity that the A functions (1) be independent of angle α, a requirement shown to hold quite well in the data of Morrison & Kronauer. This is equivalent to the proposition that a wave correlated in y would propagate throughout the boundary layer at the same angle α. Since $k = k_x \operatorname{cosec} \alpha$, correlations should therefore collapse on the more easily measured variable ωy (roughly equivalent to $k_x y$). Rigorous construction of ky requires simultaneous measurement of Δx, Δz correlations and subsequent Fourier transformation of these extensive data.

The similarity hypothesis thus suggests that the correlation coefficient $R_{uu}(y_1, y_2, \omega)$ may be reduced to dependence on two dimensionless parameters so that

$$R_{u_1 u_2} = R_{uu}(y_2^+/y_1^+, \omega^+ y_1^+). \tag{13}$$

Designating y_1 as y_{REF} the final equation requires that correlations plotted as a function of y_2^+/y_{REF}^+ with $\omega^+ y_{\mathrm{REF}}^+ =$ a constant should fall onto a single curve.

Figure 6 shows the similarity correlation of data for some values which fulfil the conditions required above and the collapse is quite good. The deviations increase as the wall is approached. This is expected since these are the regions below the log-layer where the ratio of kinematic to eddy viscosity is high and the convection velocity C_x is not equal to the mean velocity (Morrison *et al.* 1971). It is interesting that the collapse extends to $y^+ \leqslant 50$ positions since these are subject to an intensity correction procedure (Morrison & Kronauer 1969). This reinforces the previous comments that the log-layer eddies are independent of the wall even when they extend well towards it. The collapse is also good beyond the theoretical similarity limit, namely $y/a = 0{\cdot}1$ or $y^+ = 260$, confirming earlier comments about these limits.

Since Δz separations have not been used the present correlations are integrals over all k_z and hence contain a range of wave sizes, $\lambda = 2\pi/(k_x^2 + k_z^2)^{\frac{1}{2}}$. However, the $k_z \Phi(k_z)$ spectra are much narrower (about $1\frac{1}{2}$ decades) than the $\omega\Phi(\omega)$ spectra (which cover almost four decades). Hence frequency filtering along with wall distance is constraining wave size very effectively.

The similarity plot of Quad data (figure 7) is good even though the generation of Quad-correlations using second-order filters leaves something to be desired, and the r.m.s. values of the signals being correlated are much smaller, causing any system inaccuracies to be more significant.

If the Co and Quad-correlations are used to generate magnitude and phase information as described earlier, the overall correlation $M_{u_1 u_2}(\omega)$ thus obtained collapses as well as the original curves (see figure 8 which should be compared with figures 6(*b*) and 7(*b*). Figure 9 shows the phase data plotted as a function of y_2/y_{REF} for the three constant $\omega^+ y_{\mathrm{REF}}^+$ values, namely 5·3, 10·6, 31·8.

For clarity and comparison purposes we have shown the three curves as a composite (figure 10). Three features are evident.

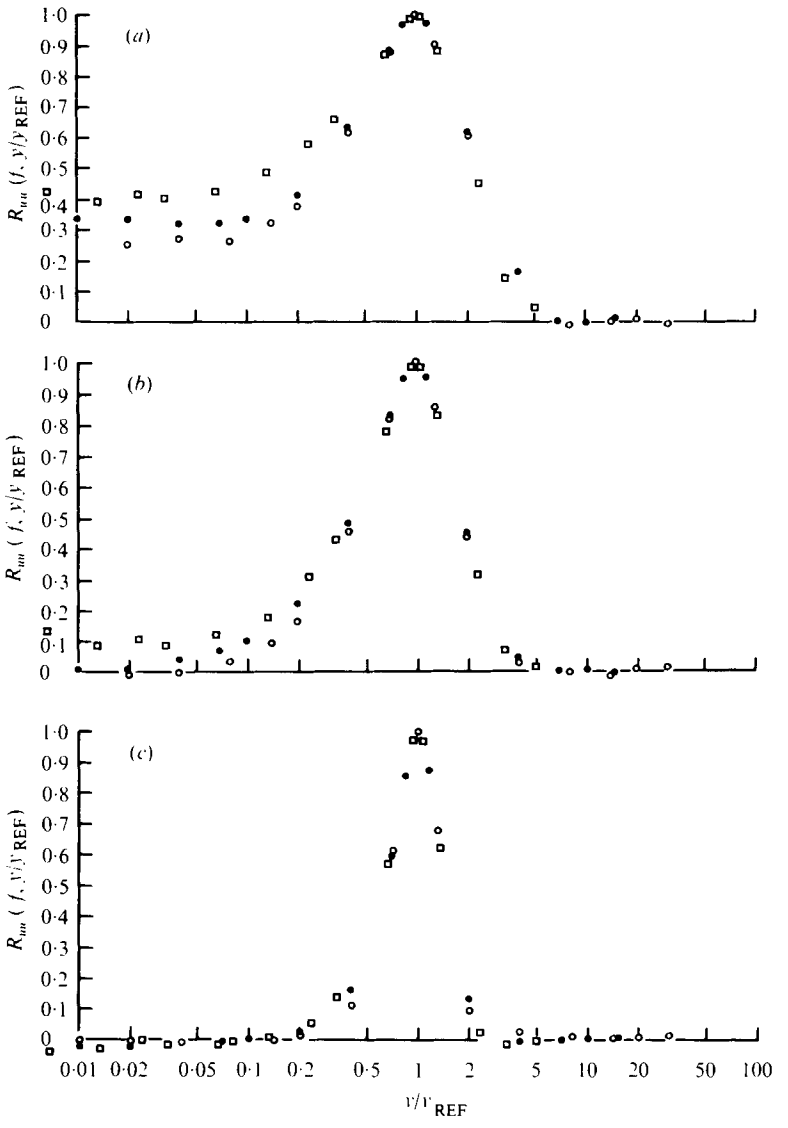

FIGURE 6. Similarity plot – Co-correlations for $\omega^+ y^+_{REF}$ = constant.

	(*a*) $\omega^+ y^+_{REF} = 5{\cdot}3$		(*b*) $\omega^+ y^+_{REF} = 10{\cdot}6$		(*c*) $\omega^+ y^+_{REF} = 31{\cdot}8$	
y^+_{REF}	f (Hz)	ω^+	f (Hz)	ω^+	f (Hz)	ω^+
300	36	○ 0·0177	72	○ 0·0354	216	○ 0·106
100	108	● 0·0531	216	● 0·106	648	● 0·318
50	216	□ 0·106	432	□ 0·212	1296	□ 0·637

(1) The phase gradient is larger for increasing values of the similarity variable, $\omega^+ y^+_{REF}$.

(2) The curve for the lowest $\omega^+ y^+_{REF}$ and $y^+/y_{REF} < 0{\cdot}1$ tends towards the asymptotic behaviour of the Co and Quad-correlations of figures 4 and 5, as previously discussed.

(3) At the highest value of $\omega^+ y^+_{REF}$ there is evidence of a phase jump occurring at a $y/y_{REF} = 2$. The value of $\omega^+ y^+_{REF}$ is 31·8 and recalling that $\omega^+ y^+_{REF} = U^+(y_{REF})\, k_x^+ y^+_{REF}$

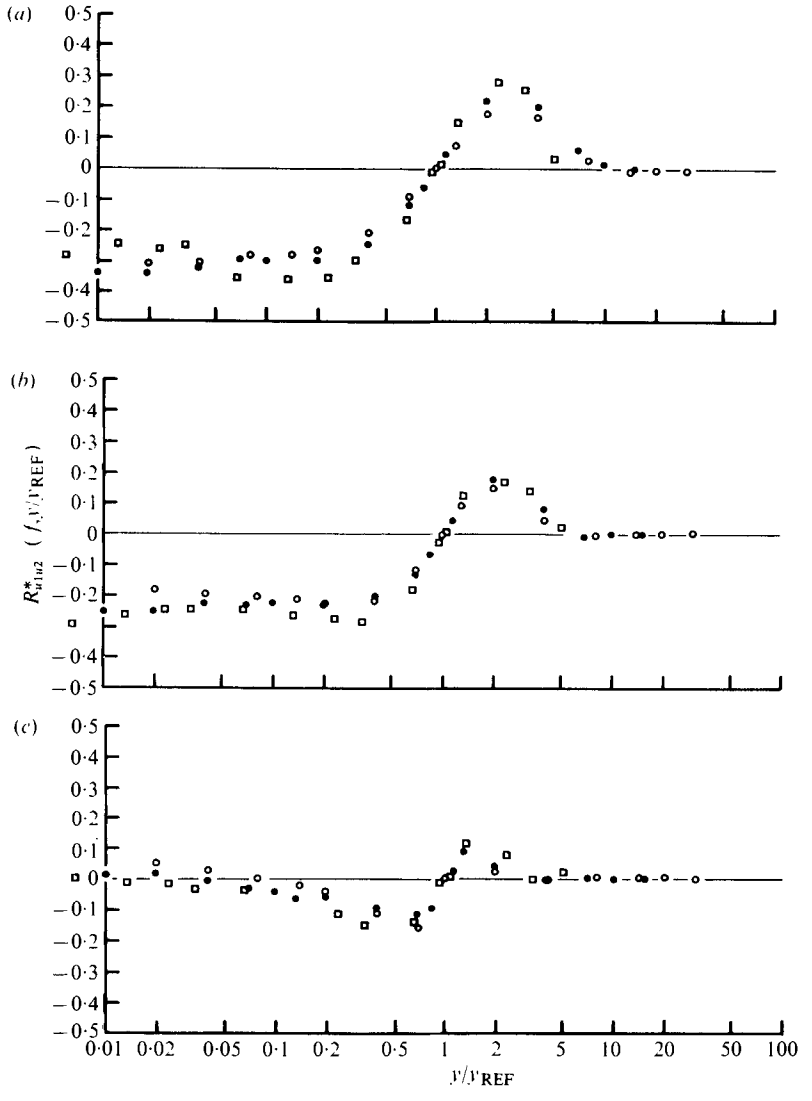

FIGURE 7. Similarity plot – Quad-correlations for $\omega^+ y^+_{REF}$ = constant.

y^+_{REF}	(a) $\omega^+ y^+_{REF} = 5{\cdot}3$		(b) $\omega^+ y^+_{REF} = 10{\cdot}6$		(c) $\omega^+ y^+_{REF} = 31{\cdot}8$	
50	216	○ 0·106	432	○ 0·212	1296	○ 0·637
100	108	● 0·0531	216	● 0·106	648	● 0·318
300	36	□ 0·0177	72	□ 0·0353	216	□ 0·106

we deduce that $k_x^+ y^+_{REF} \approx 2$. Thus the phase jump occurs at $k_x^+ y^+ \simeq 4$. This has been observed by Elliott (1972) in his phase data taken in the atmospheric boundary layer.

Morrison & Kronauer (1969) deduced that the peaks in intensity of the $\hat{u}$ and $\hat{w}$ waves are at $k^+ y^+ = 0{\cdot}6$ and $2{\cdot}4$ respectively. These values correspond to the critical layer (where wave speed matches the mean velocity) and the centre of the wave system respectively (figure 1). Hence these phenomena are interpreted as being consistent

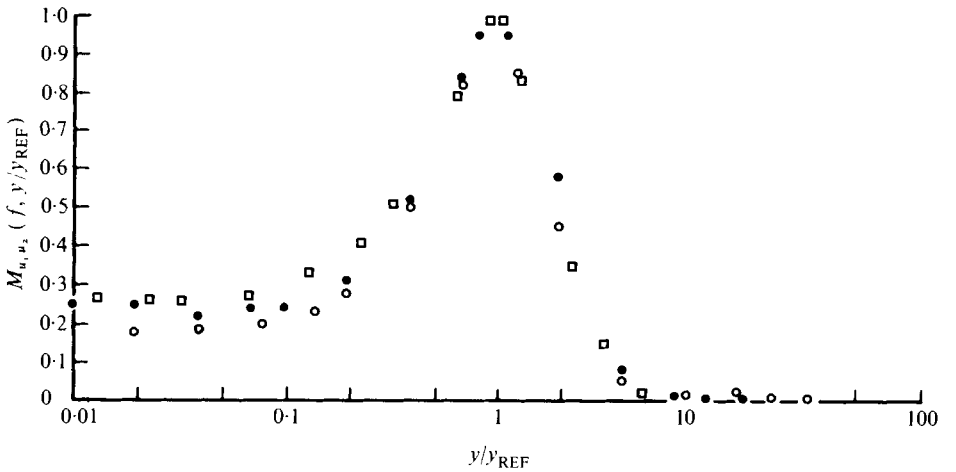

FIGURE 8. Similarity curve for filtered correlation magnitude. $\omega^+ y^+_{REF} = 10{\cdot}6$.

y^+_{REF}	f (Hz)	ω^+
50	432	○ 0·216
100	216	● 0·106
300	72	□ 0·0354

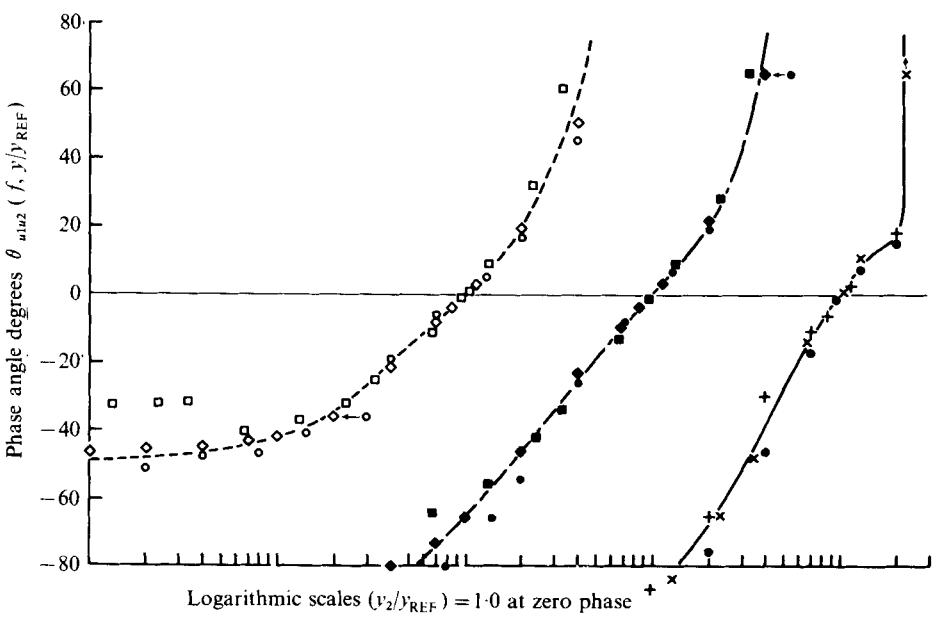

FIGURE 9. Similarity curves of phase for $\omega^+ y^+_{REF}$ = constant.

$\omega^+ y^+_{REF}$	ω^+
5·3	○ 0·106
	◇ 0·053
	□ 0·018
10·6	● 0·212
	◆ 0·106
	■ 0·0353
31·8	○ 0·637
	+ 0·318
	× 0·106

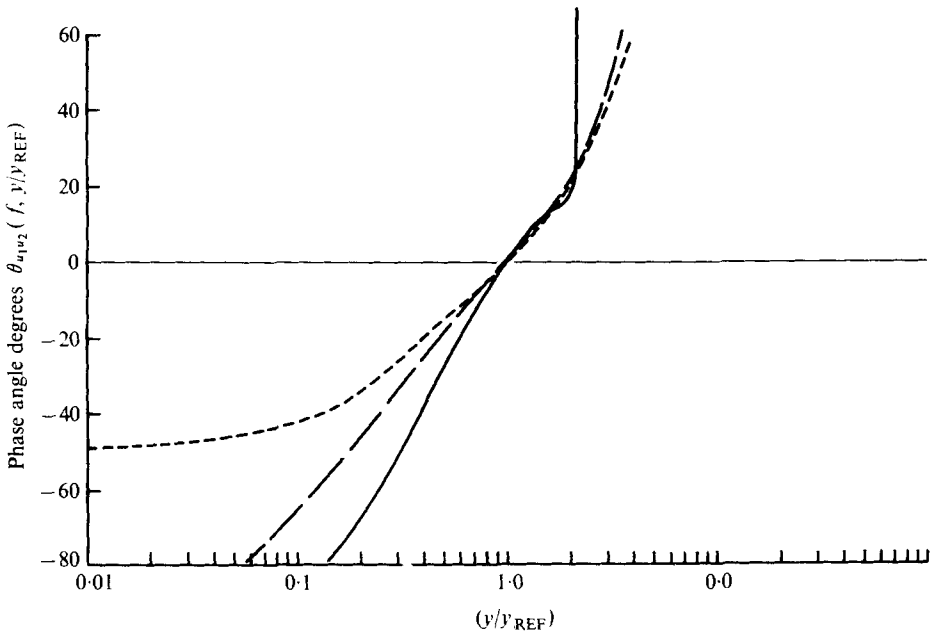

FIGURE 10. Similarity curve of phases for three values of $\omega^+ y^+_{REF}$. – – –, $\omega^+ y^+_{REF} = 5{\cdot}3$; — — —, $\omega^+ y^+_{REF} = 10{\cdot}6$; ——, $\omega^+ y^+_{REF} = 31{\cdot}8$.

with the stochastic wave model where the contributions from the $\hat{u}$ and $\hat{w}$ components vary with y. The phase jump and high phase gradient must therefore be $\hat{w}$ phenomena, whilst the lowest $\omega^+ y^+$ curve reflects the effect of the wall and is typical of $\hat{u}$ behaviour.

6. Spectra and similarity

The power spectral density functions measured for the u component as a function of y^+ for the pipe flow investigated in this experiment are shown in figure 11. The following general features may be observed.

(1) Spectra in the sublayer and buffer layer change only slowly and can be collapsed by viscous scaling (Morrison 1968).

(2) In the vicinity of $y^+ = 40$ an increasing amount of low frequency energy can be observed.

(3) In the region $200 < y^+ < 500$, this low-frequency hump predominates. In the region 70–500, this forms the well-known k^{-1} region which can be deduced, not very rigorously, from inner-layer scaling arguments.

(4) From $y^+ = 400$ and onwards, a steady decrease in the low frequency energy is observed and there is a shift up towards the previous sublayer frequency.

From such spectral curves some researchers have conjectured that a dual mixing process is at work in the boundary layer. Each stage of the process has its own frequency which is the same throughout the boundary layer, the variation in the spectrum resulting from the variation in importance of each process at different positions, y^+, in the boundary layer. However the authors wish to suggest an interpretation based on the stochastic wave model.

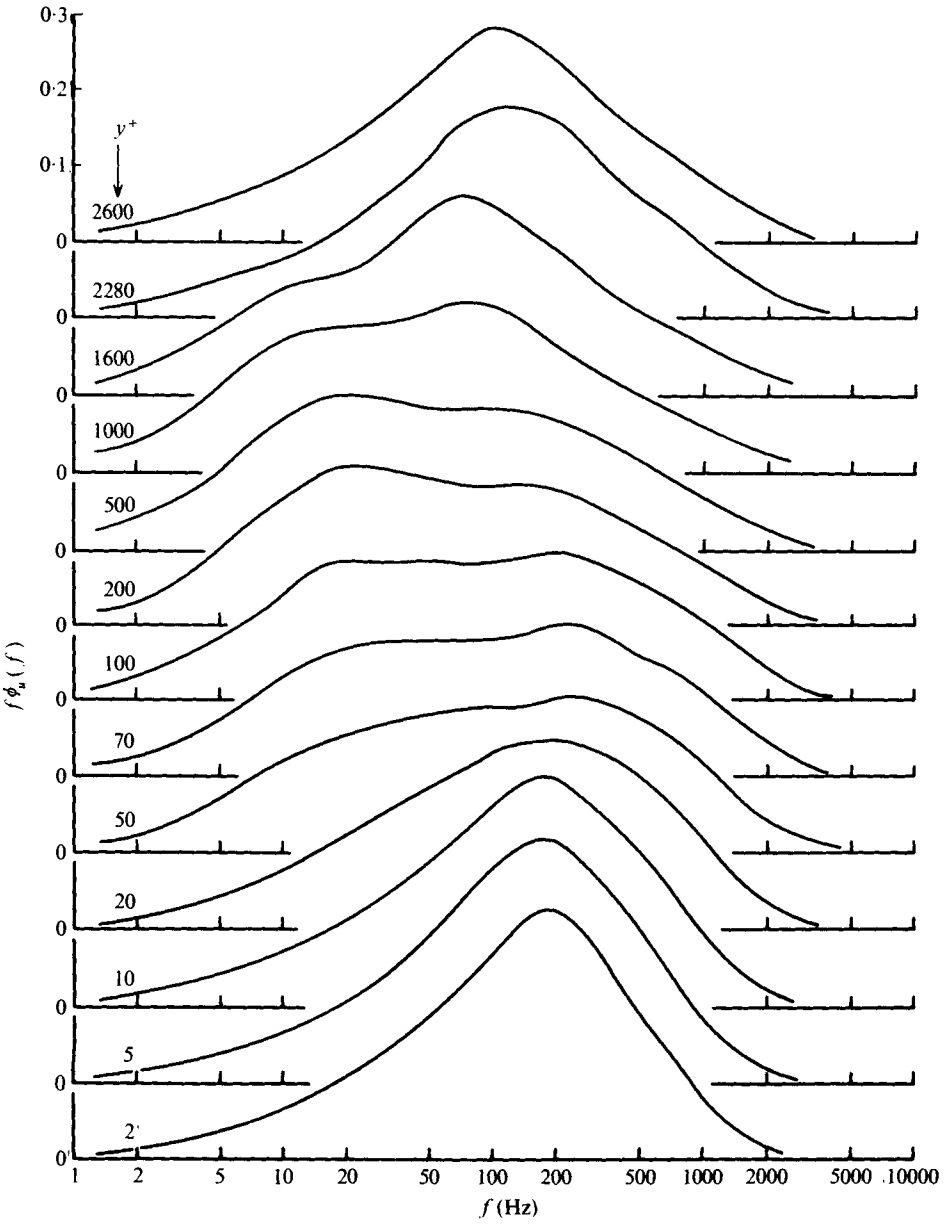

FIGURE 11. u spectra for $U_\tau = 0{\cdot}62$ m s^{-1} (2·04 ft).

Assume it was possible to measure the spectra of the natural wave components $\hat{u}$ and $\hat{w}$ (figure 1). The critical layer for the $\hat{u}$ component is given by $ky \simeq 0{\cdot}6$ while the peak intensity of the $\hat{w}$ component is further out at $ky \simeq 2{\cdot}4$. Hence y is effectively a filter on the wave size and so the spectrum obtained (for the $\hat{u}$ natural wave component) would be a mirror image of the intensity curve, i.e. with a peak at the k corresponding to $ky = 0{\cdot}6$. The same comment applies to the $\hat{w}$ spectrum only now, for the same y, the peak in k will be shifted to higher wavenumbers.

In fact it is not possible to measure the $\hat{u}$ and $\hat{w}$ spectra. The measurable u component is

$$u = \hat{u}\cos\alpha + \hat{w}\sin\alpha, \tag{14}$$

which squared gives

$$u^2 = \hat{u}^2\cos^2\alpha + 2\hat{u}\hat{w}\cos\alpha\sin\alpha + \hat{w}^2\sin^2\alpha. \tag{15}$$

The measured u spectrum is therefore a mixture of the spectra of $\hat{u}$ and $\hat{w}$, and their cross spectral density as well, integrated over all angles α.

There is not, as some authors have suggested, a large amount of sublayer size disturbances propagating out to $y^+ = 1500$. The sublayer structure and waves observed up to $y^+ = 400$ are strongly elongated in the x direction. In fact, the inclination of lines of constant phase to the stream direction is about 6° to 10°. Morrison's (1969) data showed that waves with large inclination (increasing amount of $\hat{w}$) have their u' peak much further out (about 4 times further out in ky). Hence what these spectral data are displaying at $y^+ > 400$ are waves of large inclination, probably 45° to 60°. This angle dependence can be shown by taking Δz correlations. The wavenumber k of any disturbance seen through u' data for small α depends almost entirely on k_z. However, for large α the wavenumber is more dependent on k_x or ω (which is roughly equivalent).

Thus the spectral data of figure 11 show the predominance of the $\hat{u}$ velocity component in the sublayer and a transfer to the $\hat{w}$ component in the core regions of the flow as the wave inclination angle α increases with y. Experimental evidence both in Morrison & Kronauer (1969) and McConachie (1975) shows that the proportion of $\hat{w}$ increases with increasing wall distance. The peak in $\hat{u}$ occurs at a $k^+y^+ = 0{\cdot}6$ or $\omega^+ = 0{\cdot}6C^+/y^+$ while that for $\hat{w}$ occurs at $2{\cdot}4C^+/y^+$. Now Morrison *et al.* (1971) have shown that the convection velocity (i.e. $C_x^+ = C^+/\sin\alpha$) is virtually constant in the sublayer regions. Thus as y^+ decreases, the energy spectral peak as shown with ω^+ as abscissa must increase and is limited only by viscosity. At y^+ stations in the log layer the spectral peak would be expected to move to lower and lower values of ω^+. However, this is countered by two phenomena: first, the increases in C_x^+ (which is equal to U^+ for all energetic components) and $\sin\alpha$, since U^+ and α (the angle of propagation) each increase with y. Second, and possibly the more important phenomenon, is the shift of the power from $\hat{u}$ to $\hat{w}$ components as the wall distance increases.

For lower Reynolds numbers, the low frequency peak does not occur and it appears as if sublayer disturbances are propagating right through to the core region. In fact what is occurring is that the $\hat{u}$ and $\hat{w}$ peaks are so close together as to be indistinguishable since the range of permissible wave sizes is strongly Re dependent.

Attempts were made to synthesize the spectra of figure 11. Various combinations of Gaussian signals with added periodic components invariably yielded a spectrum which was far too sharply peaked. Some theoretical correlation functions with specific properties such as zero slope at the origin were also tried but again the resulting spectra were too narrow. Success was achieved only with a combination of three spectral functions, each spectrum being that of a Gaussian distributed signal. (Log region turbulence signals are Gaussian or very nearly so.) Such a signal may be mathematically described as white noise filtered once and has a spectral function

$$\omega\Phi(\omega) = \frac{2}{\pi}\left[\frac{\omega\omega_c}{\omega^2+\omega_c^2}\right], \tag{16}$$

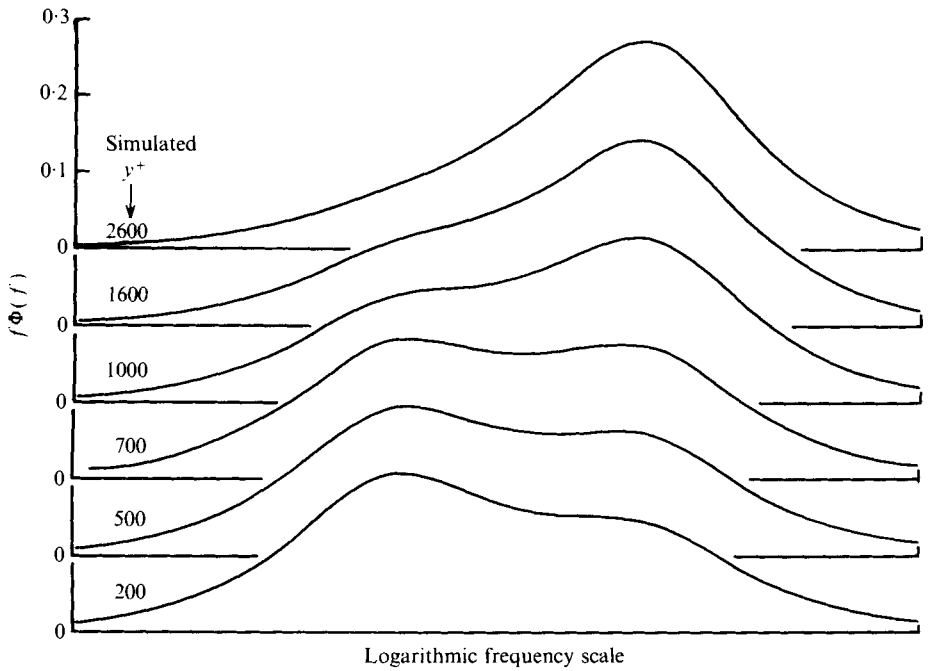

FIGURE 12. Simulated spectra for $U_\tau = 0{\cdot}61$ m s^{-1} (2 ft).

where ω_c is the corner frequency (-3 db) of the low-pass filter. This is a symmetrical bell-shaped function with a peak value of 0·32 at $\omega/\omega_c = 1{\cdot}0$. The three spectral functions to be combined are of course the postulated spectra of $\hat{u}^2$, $\hat{u}\hat{w}$ and $\hat{w}^2$ as given in (15). Hence for a particular y^+

$$\omega\Phi_{uu}(\omega) = A_1\omega\Phi_{\hat{u}\hat{u}}(\omega) + A_2\omega\Phi_{\hat{u}\hat{w}}(\omega) + A_3\omega\Phi_{\hat{w}\hat{w}}(\omega), \tag{17}$$

where, for example, $$\omega\Phi_{\hat{u}\hat{u}}(\omega) = \frac{2}{\pi}\left[\frac{\omega\omega_{\hat{u}}}{\omega^2+\omega_{\hat{u}}^2}\right],$$

and $A_1 + A_2 + A_3 = 1{\cdot}0$.

The choice of $\omega_{\hat{u}}$ and $\omega_{\hat{w}}$ may be made by considering the ratio of the location of the peak values of the similarity intensity functions, viz. $k^+y^+ = 0{\cdot}6$ for $\hat{u}$ waves and $k^+y^+ = 2{\cdot}4$ for $\hat{w}$ waves. In spectral terms the frequencies of the peaks will be

$$\omega_{\hat{u}}^+ = \frac{0{\cdot}6C_x^+ \sin\alpha_{\hat{u}}}{y^+} \quad \text{and} \quad \omega_{\hat{w}}^+ = \frac{2{\cdot}4C_x^+ \sin\alpha_{\hat{w}}}{y^+}.$$

It has already been shown that low-frequency components of u' are predominantly $\hat{u}$ waves propagating at about 6–10° while higher frequency components contain a significant amount of $\hat{w}$ waves travelling at angles of 45°–60°. Thus $\omega_{\hat{w}}/\omega_{\hat{u}} \simeq 16$–17.

It was assumed that the cross-spectral component would be centred around the arithmetic mean of the $\hat{u}$ and $\hat{w}$ frequencies.

The results of the above synthesis are shown in figure 12. The effect of y^+ was simulated by varying the proportions of $\hat{u}$ and $\hat{w}$ spectra (A_1 and A_3) entering into the composite while the amount of cross-spectral component (A_2) was kept constant at 0·1. The correspondence between the simulated and measured spectra is additional

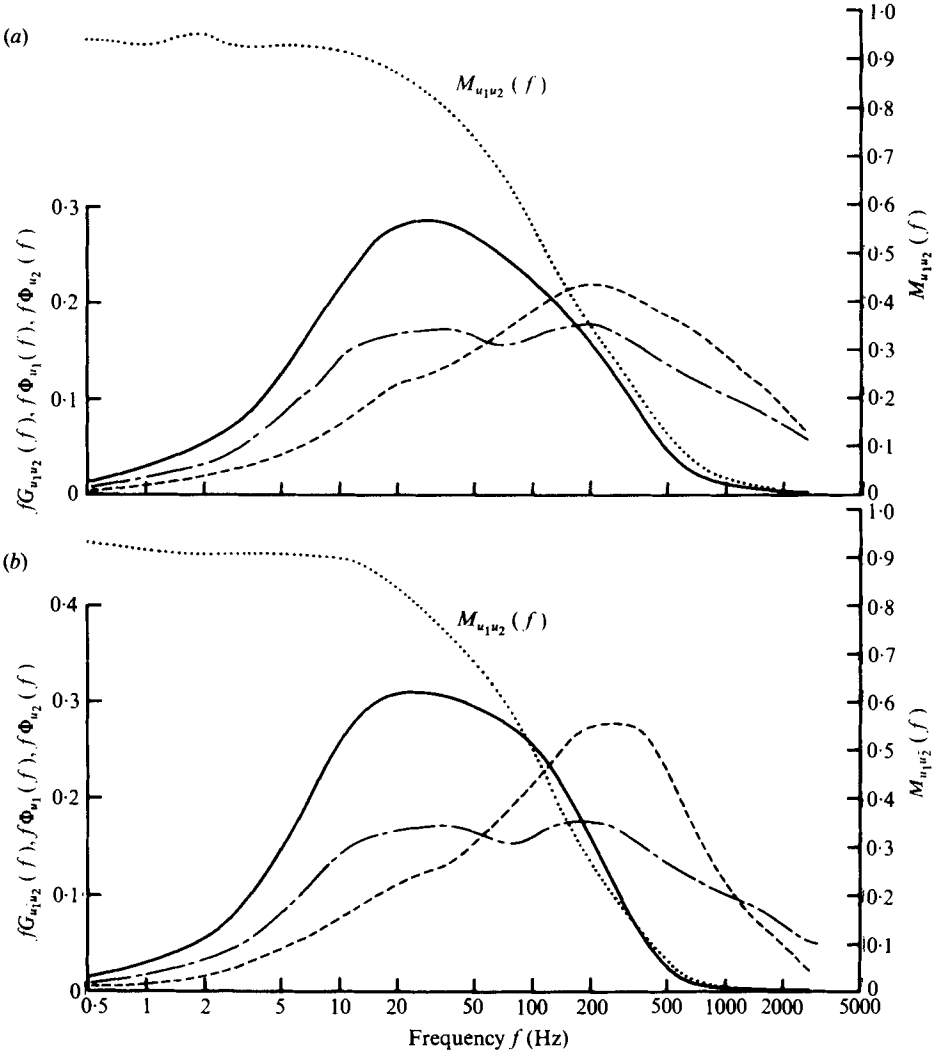

FIGURES 13 (*a*, *b*). For legend see facing page.

confirmation of the wave model. Furthermore this concept agrees with the well known fact that the spectra of the natural wave component v is single peaked.

Some cross-power spectral density curves are shown in figure 13. The data of both $y^+(4, 100)$ and $y^+(20, 100)$ of figures 13 (*a*) and (*b*) are particularly interesting as the energy distribution for u' at a y^+ of 4 and 20 is single peaked while that for $y^+ = 100$ is double peaked. However, the cross-spectral functions of $fG_{4,100}(f)$ and $fG_{20,100}(f)$ reach a maximum value at the low-frequency, log-region component of the longitudinal turbulence intensity. Thus the apparent transfer of energy across the radial separation occurs at a frequency which is controlled by the propagation of the waves in the $\hat{z}$ direction with small angles α, 6–10°. This propagation, by interacting with the mean velocity as depicted in figure 1, produces components whose size is determined chiefly by λ_z. The components of velocity in the x direction are of small wavenumber (large λ_x)

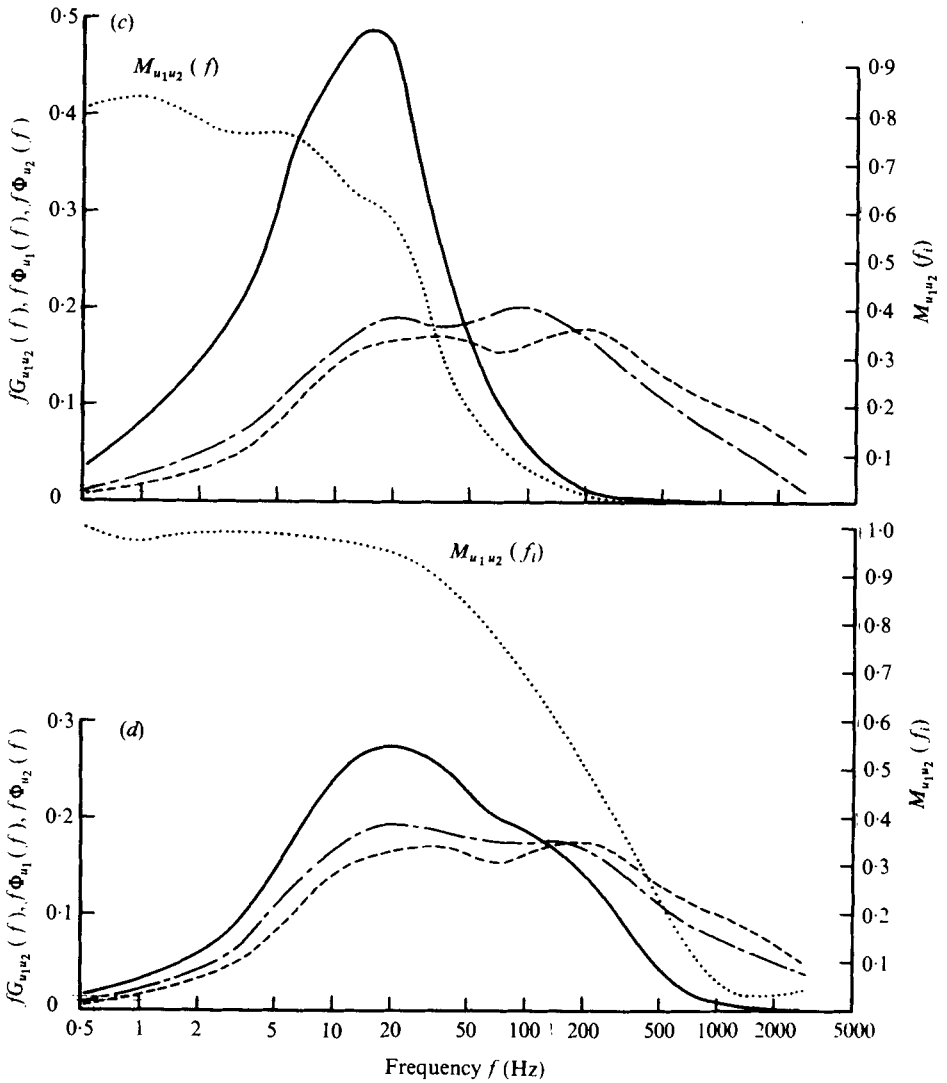

FIGURE 13. Correlation magnitudes, spectra and cross-power spectral density functions of longitudinal fluctuations in velocity.

(a)	y^+
– – – – $f\Phi(f)$	20
— — — $f\Phi(f)$	100
——— $fG(f)$	20/100
..... $M(f)$	20/100

(b)	y
– – – – $f\Phi(f)$	4
— — — $f\Phi(f)$	100
——— $fG(f)$	4/100
..... $M(f)$	4/100

(c)	
– – – – $f\Phi(f)$	100
— — — $f\Phi(f)$	700
——— $fG(f)$	100/700
..... $M(f)$	100/700

(d)	
– – – – $f\Phi(f)$	100
— — — $f\Phi(f)$	200
——— $fG(f)$	100/200
..... $M(f)$	100/200

by virtue of their small angle of intersection with the mean flow direction. In the traditionally accepted buffer and inner-log regions, the waves also cut large gradients in the velocity profile producing significant turbulent energy, i.e. the region of maximum intensity ($y^+ = 25$). These waves are highly correlated across the radial distance and this gives rise to the seemingly unusual fact that the energy transfer occurs in a frequency range where the energy density is fairly low in the near wall positions.

Proceeding outward from the wall, the two spectra merge and the cross-power spectral peak moves progressively to lower frequency and at the same time the cross-spectrum is reduced in band-width. Similarity states that the scale of turbulence is proportional to the distance from the wall. Hence this shift in the peak with wider probe separations, e.g. (100, 700) compared with (100, 200), is to be expected as the larger scales of turbulence assume greater importance with increasing wall distance.

The correlation magnitudes, $M_{u_1 u_2}(f)$ (equation 5) are also shown in figure 13. This function decreases rapidly with frequency after the peak in the cross-spectral power is passed. Although the correlation for low-frequency components is high for all y positions tested, there is very little energy transfer at a frequency of 1 Hz ($\omega^+ = 0{\cdot}00049$). In addition, the limit on the transfer of energy at the high-frequency region is probably governed by the decay in the correlation curve. This is a result of the decreasing size of the waves selected at higher frequencies.

Thus the concept that the stream function (figure 1 and the appendix of Morrison & Kronauer 1969) produces v and $\hat{w}$ components which in turn act on the mean velocity to pump $\hat{u}$ components of very large scale into the system is supported by the phase information of figure 9 (which is also the phase of $G(\omega)$) and by the cross-spectra and correlation magnitudes of figure 13.

7. Conclusion

From these measurements and related data there is emerging a coherent picture of the turbulence structure in the logarithmic region summarized in a similarity hypothesis which requires turbulence features (inclusive of others not discussed in the present paper, such as R_{uv}) to scale on wavenumber and wall distance as a product term $k_x y$. Concurrent with this scaling argument has been the use of a stochastic wave description of the fluctuating velocity components and a reduction in the dimensionality of the functions describing the phenomenon of turbulence.

The data demonstrate that large scale turbulence (small k_x) extends over a large radial region and that all these components are highly correlated. The correlations assume asymptotic values as the wall is approached. This behaviour would imply that these regions are 100 % correlated with each other and are in phase. This agrees with the National Science Foundation films of Abernathy and with other experimenters, e.g. Grass. The validity of the similarity predictions has been demonstrated in the collapse of both the correlations and the phase angles as functions of the y/y_{REF} variable even though the experimental generation of the phase data was not ideal.

The broad-band correlation data do not collapse because of the large range of wave sizes due to the lack of control on k_x. They do, however, emphasize that significant correlations exist over a large radial extent. Even for a fixed probe at a y/a of 0·12 the correlation is significant in to $y^+ = 1$. This result conflicts with the earlier data of Favre *et al.* although it agrees with Comte-Bellot's results. There is a large amount of

energy at frequencies < 16 Hz and it is possible that earlier experiments suffered from a loss of low-frequency, highly correlated, energy. In addition it is not possible to discern the traditionally accepted flow regions by examining these correlations alone.

The present measurements support the idea that the viscous regions are controlled by low-frequency log-layer fluctuations. In an attempt to determine the equivalent of an identification of the propagation of the longitudinal turbulence in the radial direction, cross-power spectral density functions were also determined for various y^+ locations and an interpretation is given. The turbulence detected by the outer probe leads that measured by the inner probe for all components.

Accurate power density spectra covering 4 decades of frequency are also presented, and analysed in the light of the similarity model which is the theoretical basis of this paper. The analysis represents a unified explanation of the spectral shapes which have been the subject of numerous speculations in the past.

This new comprehensive set of data over a large radial extent gives additional support to the Morrison & Kronauer similarity hypothesis and to the wave model described by Morrison *et al.* (1971). It is emphasized that much further careful experimentation is needed to define fully the complex relationships which exist. However, the present results have given valuable insight into the structure of pipe turbulence when interpreted in a physically consistent manner.

Professor R. E. Kronauer, of Harvard University, has in his many personal communications on wider aspects of the work of the Department in turbulence contributed greatly to this particular work.

The work has been carried out under the auspices of the Australian Research Grants Committee, which was responsible for the provision of salaries for Mr R. E. Cooper and for the financing of Professor Abernathy's visit to Queensland.

REFERENCES

ABERNATHY, F. H. 1969 *Fundamentals of Boundary Layers.* National Science Foundation Film.

BERTSCHY, J. R. & ABERNATHY, F. H. 1977 Modifications to laminar and turbulent boundary layers due to the addition of dilute polymer solutions. *2nd International Conference on Drag Reduction*, 31 August to 2 September 1977, BHRA Fluid Engineering.

BRADSHAW, P. 1971 *An Introduction to Turbulence and Its Measurement.* Pergamon.

BREMHORST, K. & WALKER, T. B. 1973 *J. Fluid Mech.* **61**, 173.

COMTE-BELLOT, G. 1969 *Aero. Res. Counc. Rep.* no. 31,609.

ELLIOT, J. A. 1972 *J. Fluid Mech.* **53**, 351–383.

FAVRE, A. J., GAVIGLIO, J. J. & DUMAS, R. 1957 *J. Fluid Mech.* **2**, 313.

FAVRE, A. J., GAVIGLIO, J. J. & DUMAS, R. 1958 *J. Fluid Mech.* **3**, 344.

FAVRE, A. J., GAVIGLIO, J. J. & DUMAS, R. 1967 *Phys. Fluids Suppl.* **10**, S138.

GRANT, H. L. 1958 *J. Fluid Mech.* **4**, 149.

GRASS, A. J. 1971 *J. Fluid Mech.* **50**, 233.

LESLIE, D. C. 1973 *Developments in the Theory of Turbulence.* Oxford University Press.

LUMLEY, J. L. 1970 *Stochastic Tools in Turbulence.* Academic Press.

MCCONACHIE, P. J. 1975 The structure of turbulence in shear flows. Ph.D. thesis, Department of Mechanical Engineering, University of Queensland, Australia.

MCCONACHIE, P. J. & BULLOCK, K. J. 1976 *J. Phys.* E **9**, 862–868.

MCCONACHIE, P. J., BULLOCK, K. J. & KRONAUER, R. E. 1977 Distribution of convection velocities in turbulent pipe flow. *Res. Rep. Univ. Queensland* no. 2/77.

MORRISON, W. R. B. 1968 Measurement of spectrum of turbulence in the wall region of pipe flow. *3rd Australian Conf. Hydraulics and Fluid Mechanics*, paper 2622. I.E. Aust.

MORRISON, W. R. B. 1969 Two-dimensional frequency–wave number spectra and narrow band shear stress correlations in turbulent pipe flow. Ph.D. thesis, Dept. of Mechanical Engineering, University of Queensland.

MORRISON, W. R. B., BULLOCK, K. J. & KRONAUER, R. E. 1971 *J. Fluid Mech.* **47**, 639.

MORRISON, W. R. B. & KRONAUER, R. E. 1969 *J. Fluid Mech.* **39**, 117.

PATERSON, R. W. & ABERNATHY, F. H. 1972 *J. Fluid Mech.* **51**, 177.

PERRY, A. E. & ABELL, C. J. 1975 *J. Fluid Mech.* **67**, 257.

SABOT, J. & COMTE-BELLOT, G. 1972 *C. R. hebd. Séanc. Acad. Sci., Paris* **275**.

TRITTON, D. J. 1967 *J. Fluid Mech.* **28**, 439.

WALKER, T. B. 1971 Analogue computation of broad-band spectra. *Rep. Dept. Mech. Engng Univ. Queensland* no. C/71.